Mass changes of Southern and Northern Inylchek Glacier, Central Tian Shan, Kyrgyzstan during ~1975 and 2007 derived from remote sensing data

Donghui Shangguan[1, 2], Tobias Bolch[2,3], Yongjian Ding[1], Melanie Kröhnert[3], Tino Pieczonka[3], Hans-Ulrich Wetzel[4], Shiyin Liu[1]

[1]{State Key Laboratory of Cryospheric Science, Cold & Arid Regions Environmental & Engineering Research Institute, Chinese Academy of Sciences, Lanzhou 730000, P.R. China}

[2]{ Department of Geography, University of Zurich, 8057 Zurich, Switzerland }

[3]{Institute for Cartography, Technische Universität Dresden, 01069 Dresden, Germany}

[4]{GFZ German Research Centre for Geosciences, Potsdam, Germany }

Correspondence to: Donghui SHANGGUAN (dhguan@lzb.ac.cn)

Abstract

Glacier melt is an important source of freshwater for the arid regions surrounding the Tian Shan. However, little is known about volume and mass changes over the last decades. In the present study, glacier area, surface elevation, and mass changes are investigated for the ~1975 - 2007 period for the Northern Inylchek Glacier (NIG) and the Southern Inylchek Glacier (SIG), the largest glaciers in the Central Tien Shan separated by the regularly draining Lake Merzbacher. The area of NIG increased by 2.0 ± 0.1 km^2 (~1.3%) in the ~1975 - 2007 period. In contrast, the SIG shrank continuously in all investigated periods since ~1975. Velocities of the SIG reached ~100 m/a in 2002/03 with a slight decrease in 2010/11. The main flow direction of SIG is towards Lake Merzbacher. The velocities at the end of the

tongue after the lake, however, are likely very low. Glacier mass balances have been calculated using multi-temporal digital elevation models from KH-9 Hexagon (1974 and 1976), SRTM3 (1999), ALOS PRISM (2006), and SPOT-5 HRG (2007). In general, a continuous mass loss for both, SIG and NIG, could be observed between ~1975 and 2007. In comparison to the ~1975 - 1999 period, mass loss in the recent decade (1999 - 2007) is slightly less negative. The dominant mass loss was observed with 0.3 ± 0.1 m w.e.a^{-1} for NIG and 0.5 ± 0.1 m w.e.a^{-1} for SIG in the ~1975 - 1999 period. We also identified a thickening at the front of NIG with a maximum surface elevation increase of about ~6 m a^{-1} between ~1975 and 1999. The thickening and area increase of NIG was due to a surge event which happened between 1990 and 1999. Furthermore, our results indicate that glacier thinning and glacier flow was significantly influenced by Lake Merzbacher.

1 Introduction

Meltwater from snow and ice is an important freshwater resource for the arid regions surrounding the Tian Shan (Sorg et al., 2012). This is especially true for the Tarim Basin in Xinjiang/Northwest China whose main artery, the Tarim River, is considerably nourished (about 40%) by glacial melt (Aizen et al., 2007; Sorg et al., 2012). The transboundary Asku River (named Sary-Djaz in Krygyzstan), originating in the Kyrgyz part of the Central Tian Shan and the main tributary of the Tarim River, contributes about 40% to the overall run-off of the Tarim River (Mao et al., 2004). On average, glacier shrinkage is lower in the inner Tian Shan than in the outer ranges (Sorg et al. 2012). The runoff of Aksu River has increased during the last decreased (Li et al., 2008; Piao et al., 2012; Liu et al., 2006). Shen et al. (2009) estimated that 13% of the annual runoff during 1957 - 2006 in the Aksu River was due to the glaciers imbalance. Reported shrinkage rates vary between ~3.7% for the entire Sary-Djaz Basin during 1990-2010 (Osmonov et al., 2013) and ~8.7% for the neighbouring Ak-Shirak Range during 1977-2003 (Aizen et al. 2006). Hence, it can be assumed that this increase is at least partly due to increased glacier melt. However, area changes show only indirect, filtered and delayed signals of climate change (Cuffey and Paterson, 2010). In addition, glaciers in Central Tian Shan are polythermal or even cold with lower mass turn-over than temperate glaciers (Aizen et al., 1997) and, hence, lower changes in area compared to temperate glaciers. However, only changes in ice thickness and mass balance can be directly linked to climate and runoff. Glacier mass balance is traditionally measured in-situ. As this work is laborious and most of the glaciers are located in remote and hardly accessible terrain, measurements can only be conducted pointwise for few glaciers. Several studies have shown that remote-sensing derived geodetic mass balance estimates are suitable to extend in-situ measurements in space and time (e.g. Berthier et al. 2010, Gardelle et al. 2013, Paul and Haeberli, 2008), and it's even used to calibrate time series of in-situ glaciological records (e.g. Zemp et al., 2013).

Glacier in the Central Tian Shan experienced significant downwasting in the last decades. Aizen et al. (2006) determined a thinning rate of -0.69 ± 0.37 m a^{-1} (or -0.59 ± 0.31 m w.e. a^{-1} mass lose, the density of converting thinning rate to mass lose was 850 kg m^{-3}) for the Ak-Shyrak Massif, the second largest glacierized massif in the Central Tian Shan, while Pieczonka et al. (2013) found a mass loss of -0.42 ± 0.23 m w.e. a^{-1} using 1976 KH-9 data and the SRTM3 DEM for several, partially debris-covered, glaciers south of Peak Pobeda/Tomür Feng (Peak Pobeda in Russian/ Tomür Feng in Chinese, it is also named after Jengish Chogsu in Kyrgyz) with a decreasing trend in the recent period (1999 - 2009). SIG, the largest glacier in the Central Tien Shan, is characterized by a layer of debris altering both rates and spatial patterns of melting. SIG was investigated in the field (e.g. with ablation measurements [Hagg et al. 2008]) and by remote sensing (especially for velocity measurements [Li et al. 2013]). However, there is still a lack of volume and mass change investigations.

In the present study we used stereo 1974/1976 KH-9 Hexagon (For ease of understanding, we unified use ~1975 KH-9 Hexagon), 2006 ALOS PRISM, and 2008 SPOT-5 HRG data and the 2000 SRTM3 DEM to assess the volume change of SIG and NIG. In addition, we investigated area changes and the glacier dynamics using also Landsat TM/ETM+ and Terra ASTER imagery.

2 Study region

Inylchek Glacier is located at the headwater of the Aksu-Tarim River Catchment in the border triangle of Kyrgyzstan, Kazakhstan and China between Peak Pobeda / Tomür Feng (7,439 m a.s.l., the highest peaks of the Tian Shan) and Khan Tengri (6,995 m a.s.l.) (Fig. 1). The glacier consists of two branches: the Southern and Northern Inylchek Glacier (SIG and NIG) which had formerly a joint tongue but glacier recession led to a separation (Kotlyakov et al. 1997; Lifton et al. 2014). The area between the two tongues was filled by Merzbacher Lake as the tongue from the SIG formed an ice-barrier which dammed the meltwater (Häusler et al., 2011). Lake Merzbacher drains almost annually in summer/autumn causing an outburst flood which can be measured up to 150 kilometres downstream with discharge peaks of up to1,500 m^3/s to 2,000 m^3/s at Xiehela hydrological station (Xinjiang/China) (Ng et al., 2007; Glazirin, 2010). SIG stretches about 60.5 km in East - West length with an area of approx. 508 km^2. NIG and SIG together account for ~32% of the total glacier area of the Sary-Djaz river basin (Ozmonov et al., 2013). The equilibrium line altitude (ELA) is located at about 4,500 m a.s.l. (Aizen et al., 2007). Existing velocity measurements of the SIG show surface velocities of about 100 m a^{-1} for the middle part of the tongue (Li et al., 2013; Nobakht et al., 2014). Interestingly, the glacier flow is mainly directed towards Lake Merzbacher (Mayer et al., 2008, Nobakht et al., 2014).

The study region is characterized by a semi-continental climate. Precipitation recorded at Tian Shan Station (years 1960 - 1997) (78.2°N, 41.9°E, 3,614 m a.s.l.) and Koilu Station (1960-1990) (70.0°E, 42.2°N, 2,800 m a.s.l.) was 279 mm a^{-1} and 311 mm a^{-1}, respectively (Reyers et al., 2013) with about 75% of precipitation occurring during summer. Hence, both SIG and NIG are mostly of "summer-accumulation type" comparable to Himalayan Glaciers (Osmonov et al., 2013). No long-term precipitation measurement exists on the glacier itself. However, a correlation between annual accumulation measured by stakes at 6,148 m a.s.l.(A_k) and annual precipitation (P) was constructed to Tian Shan Station, which was $A_k = 27.7 \bullet P^{0.61}$ (Aizen et al., 1997). The mean annual temperature at Tian Shan Station is about -7.7℃ with January being the coldest month (-21.8℃) and July the warmest (4.3℃) (Osmonov et al., 2013).

3 Data and Methods

3.1 Remote sensing datasets

Declassified Hexagon KH-9, SRTM3, SPOT-5 HRG, ALOS PRSIM, Terra ASTER and Landsat TM/ETM+ data were used to obtain information about the surface elevation, surface velocity and area extent of both SIG and NIG for different periods (Tab. 1).

The KH-9 Hexagon mission was part of the US keyhole reconnaissance satellite program whose images were declassified in 2002 (Phil, 2013). The employed frame camera system was used on a total of 12 missions between 1973 and 1980. Each scene is characterized by a spatial resolution of about 20 - 30 feet (6 - 9 m) with 240 x 120 km^2 ground coverage (Surazakov et al., 2010; Pieczonka et al., 2013). For the KH-9 missions the same film as for the KH-4 mission with a film resolution of about 85 line pairs/mm was used. In our study we used Hexagon images from mission 1209 flown in November 1974 and mission 1,211 flown in January 1976.

For the period around 2000 the unfilled finished-B SRTM version with 3 arc-second resolution (approximately 90-meter) (USGS, 2006) was used. Yang et al. (2011) and Shortridge et al. (2011) reported an absolute vertical accuracy of the final DEM of about 10 m. However, the accuracy in mountain terrain is likely worse (Gorokhovich et al., 2006; Surazakov et al., 2006; Pieczonka et al., 2011). This SRTM dataset has some data voids especially at high elevation mountainous regions due to radar shadow and layover effects (Supplementary Figure S1). Thus, parts of the accumulation regions are not entirely covered by the SRTM3 DEM. However, these gaps have been filled in the SRTM4 version using auxiliary data (Jarvis et al., 2008), but the exact time is only known for the original data. Due to the acquisition in February 2000 the DEM represents the glacier surface as constituted at the end of the 1999 ablation period. However, the penetration of the C-band radar waves of about 1 - 2 m on exposed ice and up to 10 m on dry, cold firn (Rignot et al., 2001; Gardelle et al., 2012) needs to be taken into account.

The SPOT-5 HRG instruments offer across-track stereo images with the viewing angle being adjustable through ±27° from two different orbits (Toutin, 2006). Due to the precise onboard measurements of satellite positions and attitudes of the SPOT-5 orbit, each pixel in a SPOT-5 image can be located on the ground with an accuracy of ±25 m on the 66% confidence level without additional ground control points (GCPs) (Bouillon et al., 2006; Berthier et al., 2007). The SPOT-5 HRG images are suitable for DEM generation in high mountain areas (Toutin, 2006). Thus, two SPOT-5 HRG images, acquired on 5 Feb. 2008 with an incidence angle of -9.79° and 24.94° offering a Base to Height Ratio (B/H) of about 0.63, were used for DEM generation (Tab. 1). The image contrast on the glacier of the utilized images is suitable for DEM generation, but several regions in the SPOT-5 DEM are influenced by cast shadows and were eliminated from the final DEM (see Fig. 4 & Supplementary Figure S2).

ALOS was launched in January 2006, carrying the PRISM optical sensor in a triplet mode, i.e. in forward, nadir and backward views in along-track direction (Takaku et al., 2004). We used the nadir and backward images with B/H-ratio 0.5 (Tab. 1). The horizontal accuracy of the geometrical model with Rational Polynomial Coefficients (RPC) (which contains information about the interior and exterior information) can achieve an accuracy of better than 6.0 m (or 7.5 m in horizontal direction and 2.5 m in vertical direction) without any GCPs (Takaku et al., 2004; Uchiyama et al., 2008). This accuracy can be improved by using additional GCPs.

In addition to the above mentioned imageries we used Landsat TM/ETM+ and Terra ASTER data to investigate the changes in glacier extent and to observe the glacier flow (Tab. 1). Unfortunately only SIG was covered by the utilized ASTER scenes (Fig. 3).

3.2 Glacier boundary

The glacier boundaries were delineated manually as both SPOT-5 and KH-9 are panchromatic images. Debris cover on the tongue of SIG hampered the accurate identification of the glacier margin. However, water outlets at the front of SIG and traces left after the river flow around the tongue are visible in the images. We identified the lines of the traces surrounding the debris covered ice as the glacier terminus boundary (Fig. 2a). For the NIG terminus boundary the delineation between the water and debris was used as the terminus boundary of ice (Fig. 2b). Furthermore, the hillshade based on the SRTM3 DEM provided additional information to detect the glacier boundary. The accuracy of the glacier outlines is strongly influenced by debris cover and different spatial resolutions of the used satellite datasets (Paul et al., 2013). We estimated the uncertainty using a buffer of 10 m for the KH-9 images and half a pixel for Landsat TM/ETM+ imagery (cf. Bolch et al., 2010). This led to an uncertainty of the mapped NIG area of 2.7%, 1.8%, 1.3%, 0.5% and SIG area of 1.9%, 1.3%, 0.9%, and 0.3% for the Landsat TM, KH-9, Landsat ETM+ and SPOT5 images. Under consideration of the law of error propagation, the final uncertainty was calculated using equation 1.

$$\theta_{change} = \sqrt{\theta^2_{period1} + \theta^2_{period2}} \qquad (1)$$

Where $\theta_{period1}$, $\theta_{period2}$, θ_{change} represent the uncertainties of glacier in period1, period2 and change

The uncertainties for SIG (NIG) changes are 2.3% (3.2%) between ~1975 and 1990, 2.1% (3.0%) between 1990 and 1999, 0.9% (1.4%) between 1999 and 2007, and 1.3% (1.9%) between ~1975 and 2007.

3.3 Flow velocity of SIG

To investigate the dynamic behaviour of the SIG, we measured glacier velocity rates using multi-temporal optical satellite imagery covering a time span of about one year. Using the EXELIS VIS ENVI Add-on COSI-Corr, a frequency based feature tracking (phase correlation) was performed in order to get the horizontal offset of corresponding image points. The tracking was performed using the method of phase correlation implemented in Cosi-Corr For ASTER data a previous subpixel-coregistration was done as described in Leprince et al. (2007) using the gap-filled SRTM3 DEM as vertical reference. Landsat data were assumed to be quasi-coregistered because of the same sets of GCPs and vertical references used for orthorectification. Dependent on to an expected annual average velocity of SIG of up to 90 m/a (observed in 2003/2004 [Mayer et al., 2008]) and the images' resolution, the step size was

4 px for ASTER and 2 px for Landsat, so both displacement maps have a final resolution of 60 m.

The relative offsets of the co-registered images show the phase difference of the previously Fourier transformed input data and can be estimated by the correlation maximum (Leprince et al., 2007). For the 2010/2011 observation period, offsets in the north-south- and east-west-direction were measured with an accuracy of 1/7 px using quasi coregistered Landsat TM (L1T) data. For the 2002/2003 period, we achieved a precision of 1/4 px based on 1/25 px-coregistered ASTER (L1A) data. The reliability of the displacement vectors was assessed by the ratio of the RMSE and the resolution of the respective input data. Beside SIG , velocity field were also derived for adjacent glaciers. The calculation of the RMSE values takes SIG observations into account. Therefore, the survey compasses a huge amount of significant and non-significant velocity measurements, which allows a solid reliability assessment. Beforehand, errors caused by clouds, topography and low image contrast have been removed from the matching result. The final uncertainty has been determined with 0.25 m/a for 2002/2003 and 0.47 m/a for 2010/2011.

3.4 DEM generation and DEM postprocessing

KH-9, ALOS PRISM and the SPOT-5 HRG data were processed using the Leica Photogrammetry Suite (LPS), vers. 2013 with the UTM WGS84 reference system.

For the stereo processing of the KH-9 images, we measured 38 GCPs for the DEM covering the lower part of Inylchek Glacier and 47 GCPs for the stereopair covering the accumulation region of Inylchek Glacier with a final RMSE of ~1 m. GCPs coordinates and elevations were derived from Landsat 7 ETM+ scenes and the SRTM3 DEM. For the processing the frame camera model in LPS was used and the final resolution of the KH-9 DEMs was 25 m.

ALOS PRISM and SPOT-5 were processed with four additional GCPs in order to improve the accuracy of the exterior orientation (Supplementary Table S1). The automatically generated tie points (TPs) were visually checked in terms of ground objective and topographic features. In total, 120 TPs were used. The spatial resolution of the ALOS and SPOT-5 DEM was 10 m. Differencing of multi-temporal DEMs necessitates a co-registration including the removal of horizontal and vertical offsets (Pieczonka et al. 2013). We used the analytical method proposed by Nuth and Kääb (2011) which has been proven to provide robust results and to be computationally effective (Paul et al. 2014). All DEMs were bilinearly resampled to the same cell size of 30 m. The resolution is a compromise between the possible higher resolution of KH-9 and SPOT-5 DEMs and the lower resolution of the SRTM DEM. The shift vectors were calculated based on selected ice free sample regions (Supplementary Figure S3). The resulting horizontal shifts were in the order of 2 pixels and the z-offsets varied between 1.3 m and almost 20 m (see Table 2).

3.5 DEM uncertainty

The accuracy of the final DEM differences was evaluated with regard to the vertical offset over ice-free terrain which is supposed to be stable. Additionally, we evaluated the DEMs by GPS surveys. Outlier values for the 1999 - 2007 periods were identified by 3σ and excluded from further processing (cf. Gardner et al., 2013; Gardelle et al., 2013). For the period ~1975 - 1999 and ~1975 - 2007, in order to omit high values due to the glacier surge, outliers were defined and excluded as follows: all values larger than the sum of the maximum elevation difference (which is larger than 3σ) in the surging region, standard deviation and mean of the elevation difference. After outlier cleaning several obvious errors could still be detected in the accumulation regions. According to annual snow-firn layers (less than 275 mm/year) at 6,148 m a.s.l. on SIG from 1969 to 1989 (Aizen et al., 1997), the maximum accumulation can be inferred to be less than 9.1m (275mm/year * 33years) for the period ~1975 - 2007. In addition, the seasonal snow depth was calculated with a maximum of 9.0 m by comparison with the SRTM C-band and SRTM X-band (See below). In this case, a threshold of 20 m as the maximum accumulation was used for elevations above 4,000 m a.s.l..

The uncertainty of the DEM differences was estimated by the normalized median absolute deviation (NMAD) (which was expressed by $1.4826 * MED(|\tilde{x} - x_i|)$, x_i: elevation difference; $\tilde{x}$:Median) in the ice free terrain (see Table 2).

NIG and SIG were covered by snow as revealed by a Landsat ETM+ (Level 1) scene from 18 February 2000 which was used to infer the snow condition at the time of the SRTM mission 11 - 20 February 2000. The C-Band (6 GHz) allows penetration under dry snow conditions whereas the penetration of the X-band (10 GHz) is considered to be negligible (Gardelle et al., 2012). Hence, we compared the SRTM-C-band and SRTM-X- band DEMs to estimate the radar penetration (Gardelle et al., 2012). Both DEM cover SIG and NIG and were resampled to 30m resolution. The result showed that the mean elevation difference varies between 1.7 m in the lower debris-free ablation area and about 6.0 m in the higher accumulation area according to each altitude zone (100 m) with a maximum elevation difference of about 9 m (Supplementary Figure S3), which was discrepancy with the penetration (9 m at 4,500 m a.s.l.) in Akshiirak massif by using a linear method (Surazakov et al., 2006). The uncertainty of the radar penetration (*e*rp) was estimated by the Standard Deviation (STD) to be 1.9 m. It was assumed that the possible slight penetration of the x-band radar beam is within this uncertainty range. The uncertainty of the DEM differences was calculated according to equation 2.

$$e = \sqrt{\mathrm{NMAD}^2 + erp^2} \qquad (2)$$

The biases of different DEMs in stable and non-glacierized regions after co-registration are shown in Table 2.

In order to validate the accuracy of the DEMs, we randomly collected six Differential GPS points measured with Uni-Strong GPS-RTK in 2010. Among the GPS points, three were located on the debris covered glacier part, two were located on ice-free terrain and one was on the glacier surface (Table 3). The mean difference between GPS and SPOT-5 DEM was -8.2 m with a standard deviation of 6.6 m before co-registration. After co-registration of SPOT-5 DEM with SRTM3 (master DEM), the mean offset was -0.4 m with a standard deviation of 5.7 m. However, we cannot evaluate the bias of ablation in the debris covered region and the glacierized region between 2008 and 2010 and we also cannot evaluate the bias from the points by GPS in comparison to the DEMs cell size. In order to analyse the relative uncertainty of the ALOS DEM compared to the SPOT-5 DEM we additionally measured a profile with 342 sample points between 3,050 and 3,350 m a.s.l. on the glacier. The results showed that the uncertainty is 4.5 m with a standard deviation of 3.6 m. This uncertainty included the glacier melt and glacier elevation changes between 2006 and 2007.

3.6 Glacier elevation change and mass balance

The elevation change from DEM differences was calculated based on the area-average value per 100 m elevation zone (cf. Xu et al., 2013; Gardner et al., 2013, Formula 2, Figure S2). Data voids typically caused by low image contrast (e.g by cast shadows) for optical data, radar shadow and layover for microwave data, and as a consequence of outlier filtering, there are missing values in each zone. Thus, the mean volume of each zone will be used to calculate the elevation change.

$$\Delta h_{gl} = \frac{\sum_{i=1}^{n} \Delta h_i * s_i}{s_{all\ zones}} \qquad (3)$$

where i is the number of zones, Δh_i is mean glacier elevation change in the respective zone after radar penetration correction, s_i is the area of each zone, n is the total number of zones, and $s_{all\ zones}$ is the total area of all zones. The distal part of the tongue of SIG, which is not covered by the SPOT-5 DEM (Fig. 1), was filled with the ALOS DEM. In order to account for the different times of image acquisition of ALOS PRISM and SPOT-5 we used the elevation change per year for gap-filling. The average elevation change (Table 5) was calculated by multiplying the annual average elevation changed with the time span. Where there was a lack of altitude zones (zones of 6,800 - 7,100 in SIG and 6,500 - 6,700 in NIG), we have used the maximum elevation change, minimum elevation change and an half of minimum and maximum elevation change to interpolate that lack according to Figure 6. However, there are few weights of area for those regions (cf. supplementary figure 2), it is not sensitive for calculating mass balance by using Area-average mass balance and could be omitted. A density of 850 ± 60 kg m^{-3} was used to convert our surface lowering rates (dh/dt) to actual mass change rate (MB/dt) (cf. Huss, 2013).

The final mass balance uncertainty (E) has been calculated considering the DEM uncertainty (NMAD), the snow/ice density uncertainty (ρ), and the radar wave penetration uncertainty (erp) (Equation 4).

$$E = \sqrt{NMAD^2 + erp^2 + \rho^2} \qquad (4)$$

4 Results

4.1 Glacier flow

We noticed high velocities with an average flow of about 120 m/a (between point b and point c) for the SIG towards Lake Merzbacher while the remaining part of the debris-covered tongue (between point a and point b) has significantly lower velocities with decreasing rates from point b to a and has likely stagnant parts (Fig. 3). Hence, the main flow direction of the tongue is towards Lake Merzbacher and not to the end of the glacier tongue. Most tributaries have active flows until the confluence of the glacier with velocities varying typically between 30 and 60 m/a. The general patterns and velocities in main flow direction are similar for both investigated periods (2002/03 and 2010/11). However, there are discrepancies in region 1 and region 2 where we found high velocities for the period 2002/03 and lower velocities for the 2010/11 period (Fig. 3). Comparing the velocities of 2002/03 and 2010/11 shows a slight decrease for the main stream of SIG (Supplementary Figure S5).

4.2 Glacier area change

The SIG shrank continuously by about 0.1 ± 0.1 km^2, 0.5 ± 0.1 km^2 and 0.2 ± 0.1 km^2 during the periods ~1975 - 1990, 1990 - 1999, and 1999 - 2007. The overall area loss of the SIG was 0.8 ± 0.1 km^2 during ~1975 and 2007, accounting for ~0.2% of its area in ~1975. The NIG lost an area of 1.2 ± 0.1 km^2 during the period ~1975 - 1990 followed by an increase in area of 3.7 ± 0.1 km^2 (1990 - 1999). During this period the glacier showed a strong advance of about 3.5 km. The glacier shrank again by 0.4 ± 0.1 km^2 in the consecutive period (1999 - 2007). Overall, the area of the NIG increased by 2.0 ± 0.1 km^2 during ~1975 - 2007, accounting for ~1.3% of its area in ~1975 (Fig. 2; Tab. 4). Consequently, the area of the entire Inylchek Glacier system increased by 1.3 ± 0.1 km^2 (~0.2%) between ~1975 and 2007.

4.3 Glacier mass change

Both SIG and NIG experience a mass loss (0.3 ± 0.1 m w.e.a^{-1} and 0.4 ± 0.1 m w.e.a^{-1}) between ~1975 and 2007 (Fig.4c & Tab. 5). For the ~1975 - 1999 period, the mass loss of SIG and of NIG was about 0.3 ± 0.1 m w.e.a^{-1} and 0.5 ± 0.1m w.e.a^{-1}, respectively. After 1999, a mass budget of -0.3 ± 0.4 m w.e.a^{-1} was measured for NIG while SIG showed decelerated mass loss or even a possible balanced budget of -0.1 ± 0.4 m w.e.a^{-1}. We also noted that the elevation thinning at the dam in the SIG was higher (1.0 - 2.0 m a^{-1} from ~1975 to 2007) (Fig. 4). Higher flow was shown in Figure 3 and it would cause more ice to be transported to this part (Ng et al., 2007; Mayer et al., 2008). Thus, the significant elevation thinning of this part could be related to Lake Merzbacher.

The analysis elevation differences measured along the main flowline (Fig. 5) allows more detailed insights into the characteristics of the glaciers behaviour. For the SIG almost all parts of the glacier tongue showed a surface lowering for the periods ~1975 - 1999 and 1999 - 2007 (from glacier tongue to point b, Fig. 5). There are large amplitudes in elevation change between point a and b (Fig. 5) which is due to the heavily debris-covered part below Lake Merzbacher with low or even insignificant flow velocities (Fig. 4). Between point b and c a clear surface lowering could be observed for the period ~1975 - 1999 while a slight decrease with small amplitudes could be measured for the period 1999 - 2007 (Fig. 4 and Fig. 5). We also identified that parts of the elevation changes are positive above point c for 1999 - 2007 (Fig. 4a) which was shown up to the length of 37,000 m (see Fig. 5 SIG). And an apparent elevation increase at a mean rate of 1 - 2 m a^{-1} was observed for the period 1999 - 2007 in region 2 of the accumulation region in SIG (Fig. 4a) where the velocity was also faster measured in 2002/2003 (Fig. 3a). It looks like a tributary surge. In contrast, NIG showed a clear thickening with maximum values of ~6 m a^{-1} around point d for the period ~1975 - 1999 while a rapid thinning of ~4 m a^{-1} was measured between point e and f. The elevation change showed a decreasing trend from point d to point f for the period ~1975 - 1999. Thereafter, between 1999 and 2007 the elevation change increased from point d to point f. Taking the strong advance between 1990 and 1999 and the retreat between 1999 and 2007 into account (Fig. 3), it can be assumed that NIG was surging during 1990 and 1999. Consequently, mass was transferred from the accumulation region to ablation region between ~1975 and 1999 (Fig. 4b).

Surface lowering for SIG in the 1999 - 2007 period was measured a.s.l. with a mean rate of about 0.7 ± 0.5 m a^{-1} below 4,300 m a.s.l.. Meanwhile, thickening was observed above 4,300 m a.s.l. with a mean rate of about 0.16 ± 0.5 m a^{-1}. This shows that SIG experienced likely a slight mass gain in the accumulation region in the recent decade (Fig. 6). For the period ~1975 - 1999 SIG experienced a thinning below 4,800 m a.s.l. and a slight thickening above elevation of 4,800 m a.s.l.. The obvious thinning was observed at zones of 3,700 - 4,500 m a.s.l. and zones of 5,400 - 5,800. For the period ~1975 - 2007, the elevation of the SIG was thinning under 4,800 m a.s.l.. It indicated that the surface thickening between zones 4,300 and 4,800 for period 1999 - 2007 is small and cannot offset the surface thinning for period ~1975 - 1999. For the NIG, it is different in more or less all altitudes due to its surge-type behaviour. However, Compared to elevation changes in the same altitude of SIG for the 1999 - 2007 period, NIG experienced higher mass loss between e 3,300 - 3,600 m a.s.l. (2.0 ± 0.5 m a^{-1}) than SIG (0.9 ± 0.5 m a^{-1}). Consequently, the stronger thinning at the tongue in comparison to SIG could be due to the quiescent phase after the surge.

5 Discussion

Osmonov et al. (2013) reported an average shrinkage of 3.7 ± 2.7% from 1990 to 2010 with 10 advancing glaciers in the upper Aksu Catchment. The glacier retreat in adjacent regions varied between 3.3% in Aksu River (China) and ~30% in valleys of Zailiyskiy and Kungey Alatau during the last decades (Bolch, 2007; Aizen et al., 2006; Liu et al., 2006) with highest shrinkage rates in the outer and more humid ranges and the lowest in the inner and drier ranges (Sorg et al. 2012, Narama et al. 2010). In western China, including the Chinese part of the Tian Shan, more than 80% of the glaciers were retreating and only some glaciers are in an advancing phase for the period 1965 to 2001 (Ding et al., 2006). Our study revealed only a slight retreat of SIG during ~1975 and 2007 while a strong advance for NIG could be identified between 1990 and 2000. Our results tend to be in agreement with Osmonov et al. (2013) who, however, did not analyse SIG and NIG separately and did not reported the NIG surge.

Our observed velocities for SIG (~120 m a^{-1} for the main tongue) are in agreement with Nobakht et al. (2014) who measured values of 0.3 - 0.4 m day^{-1} (~100 - 150 m a^{-1}) based on ASTER and Landsat data, but larger than the 0.2 m day^{-1} (~75 m a^{-1}) noted by Li et al., 2013 based on ALOS PALSAR data. The velocity close to Lake Merzbacher in the period 2003/2004 (75 - 90 m a^{-1}) is also in agreement with in-situ measurements (80 - 90 m a^{-1}, Mayer et al., 2008). Glacier calving could be observed for the SIG with mean velocities of up to 0.4 m day^{-1} between 2009 and 2010 (Nobakht et al., 2014). Furthermore, there was a huge mass loss in the periods ~1975 - 1999 and 1999 - 2007 near the lake dam. Flow velocities at the middle part of the SIG tongue (between point b and c) were higher than at parts (between points a and b, Fig. 3). High velocities transports mass from upstream and offset the mass loss due to ice melt. Furthermore, the lake enhances melt and causes calving. The water likely also lubricates the glacier base bed. Hence, the lakes likely causes the high velocity until the lake margin and influences the ice dynamics (cf. Mayer et al. 2008) and the mass change of a glacier.

One of the major uncertainties in our study is caused by low coverage of reliable data in several altitudinal zones in the accumulation regions of both glaciers. Pieczonka et al. (2013) used figures based on vision inspection to make up the short samples in accumulation regions. In this study, the maximum, minimum and middle elevation changes were used to interpolate that lack. We found that the area weight of samples in those zones were too small (0.5% above 6,500 m a.s.l. in area) to effect the results (It brings about 0.005 – 0.02 m a^{-1} uncertainty) (Supplementary Fig. 2). And the times of KH-9 images are not the same; it could be brought uncertainty though we used annual elevation changes to calculate mass balance. In addition, we did not consider the seasonal correction because those DEMs are from winter.

Geodetic mass balance measurements of 12 mainly debris-covered glaciers south of Pik Pobeda/Tomur Peak close to our study area revealed that most of the glaciers have been losing mass with rates between 0.08 ± 0.15 m w.e. a^{-1} and 0.80 ± 0.15 m w.e. a^{-1} for the time period 1976 - 2009 (Pieczonka et al., 2013) and two glaciers gained mass and one glacier (Qingbingtan Glacier No.74) showed signs of a surge similar to NIG. The mass loss was lower during the last decade (1999 - 2009) than before ~1975 (Pieczonka et al., 2013). This tendency is in line with our results for both SIG and NIG where we found on average a clear mass loss during 1975 - 1999 followed by a decreasing mass loss between 1999 and 2007. Existing in-situ mass balance measurements in the Tian Shan also showed clearly negative mass budgets since the beginning of the measurements in the 1960s (WGMS 2013; Sorg et al. 2012). Such as, the mass balance from Karabatkak and Tuyuksu was -766 mm a^{-1} and -586 mm a^{-1} from 1974 - 1990, respectively (Unger-Shayesteh et al., 2013; Cao, 1998). However, it is disagreement on the mass balance of the Urumqi Glacier No.1 where the mass balance of the Urumqi Glacier No.1 was -0.14 m w.e. a^{-1} during 1958 - 1996, and -0.71 m w.e. a^{-1} during 1996 - 2009 (Wang et al., 2012). Further studies based on ICESat laser altimetry pointed out that, on average, glaciers in the Tian Shan underwent clear mass loss between 2003-2009 (-0.58 ± 0.21 m w.e. a^{-1}) (Gardner et al. 2013). And the mass loss in lower altitude of SIG is less than in higher altitudes (red is more negative) derived from the two ICESat profiles. Comparison with our result, it is adverse in this region.

The obtained characteristics with a clear thickening at the tongue of NIG and a lowering in higher altitudes (Fig. 5) together with the data of area and length change are a clear indicator for a surge event that happened between 1990 and 1999. Surging glaciers in the Tian Shan were also reported by Narama et al. (2010), Osmonov et al. (2013), Pieczonka et al. (2013) and, in earlier times by Dolgoushin and Osipova (1975), hence this phenomenon is also not infrequent in the Tian Shan. The surge event of the NIG probably happened in late 1996 with an advance of about two kilometres (Maylyudov (1998) cit. in Häusler et al. 2011). However, it was a non-typical surging event due to the lack of surge characteristics such as: areas of stretched ogives, erosion scars, transverse crevasses or breaching structures; Hodkins et al. (2009) described this phenomenon as partial surges. Furthermore, a significant surface elevation increase of a southern tributary (region 2 in Fig. 4a) in the period 1999 - 2007 provides evidence for a tributary surge. This finding is corroborated by clearly lower velocities in 2011/12 than before. Cuffey and Paterson (2010) pointed out that mass displacement down-glacier is an important signal that occurs before a glacier surge. Their results also showed that glacier surging will re-distribute glacier mass.

Both parts of the ablation regions of the SIG and NIG are covered by debris below ~ 3,500 m a.s.l. The surface of SIG showed considerable thinning rates but also great variability for both investigated time periods of ~1975 - 1999 and ~1975 - 2007. The surface lowering is higher at the frontal part of the tongue despite thick debris cover. This is likely due to low flow velocities or even stagnancy was found. This is in line with several other studies which found significant mass loss despite debris cover (Bolch et al. 2011, Kääb et al. 2012, Nuimura et al. 2012, Pieczonka et al. 2013). Field based measurements in 2005 of moraine thickness and ablation rates on the SIG revealed a dependency of ablation upon debris thickness with ablation rates from 2.8 to 6.7 cm/day with a mean of 4.4 cm/day (Hagg et al., 2008). The lower velocities and even immobility below Lake Merzbacher indicate that there was little mass supplied from upstream. Therefore, the significant mass loss can be explained by the influence of backwasting at ice cliffs and melting at supraglacial ponds (Fujita & Sakai, 2009; Han et al., 2010; Juen et al. 2014) but likely also to be due to reduced glacier flow from the accumulation region (Quincey et al. 2009; Schomacker, 2008; Benn et al., 2012).

Measurements at the Tian Shan Station (3,614 m a.s.l.) located 120 km west of SIG suggested that both increasing temperature and decreasing precipitation were detected during the ablation season (May-September) for the period 1970 - 1996; and a decreasing temperature and slight decreasing precipitation was also found in the ablation season for the period of 1997-2009 (Osmonov et al., 2013; Krysanova et al., 2014; Reyers et al., 2013). It is disagreement on climate change in Tarim Basin where temperature increased after 1985 and annual precipitation increased after 1980 (Shi et al., 2006; Chen et al., 2009). Hence, the observed significant glacier mass loss between ~1975 and 1999 is most likely a consequence of the ablation season warming and precipitation decrease which led to an accelerated melting and less accumulation. Reduced mass loss or even the possible balanced condition between 1999 and 2007 can likely be explained by reduced ablation due to temperature decrease.

6 Conclusion

We investigated the velocity, glacier area, surface elevation, and mass changes of SIG and NIG) for the ~1975 - 2007 period based on multi-temporal space-borne datasets sources such as KH-9 Hexagon, Landsat, and SPOT-5 HRG data. Our results show that SIG has a velocity of about 100 m a^{-1} for large parts of the tongue with a main flow direction towards Lake Merzbacher and low velocities with likely stagnant parts at the terminus below the lake. It was also noted that the velocities at the SIG tongue in 2002/2003 compared to 2010/2011 showed decreasing tendencies. In general, the area of the entire Inylchek glacier system decreased in the ~1975 – 2007 period, however, NIG was surging between 1990 and 1999 which caused an overall area increase of 2.0 ± 0.1 km^2 (~1.3%) between ~1975 and 2007. The generated DEMs from ~1975 and 2007 were of good quality though partial missing information in the accumulation regions resulted in higher uncertainties. The results showed that the mass balance of both SIG and NIG was negative from ~1975 to 2007 despite the surge of NIG in the 1990s. A tributary surge was disclosed during 1999 and 2007 at SIG. The amplitude of both glaciers' mass loss is different. For NIG a mass balance of about -0.3 ± 0.4 m w.e.a^{-1} was measured for all investigated time periods. SIG, on the other hand, revealed decreasing mass loss in the recent decade. The overall mass loss for SIG was 0.4 ± 0.1 m w.e.a^{-1} between ~1975 and 2007.

Despite debris cover, surface lowering is highest at the distal part of the tongue of SIG where also low velocities are prevailing. The elevation thinning at the lake dam was shown to be quicker likely caused by calving into Lake Merzbacher and the flow remained high until the calving front. Thus, glacier thinning and glacier flow is significantly influenced by the lake.

Acknowledgements

This work was supported by the Ministry of Science and Technology of the People's Republic of China (Grant 2013CBA01808); State Key Laboratory of Cryospheric Sciences (SKLCS-ZZ-2012-00-02); the National Natural Science Foundation of China (Grant: 41271082 & 41030527); the CAS Strategic Priority Research Program-Climate Change: Carbon Budget and Relevant Issue (Grant No. XDA05090302), German Research Foundation (Deutsche Forschungsgemeinschaft, DFG, code BO 3199/2-1) and the German Ministry of Education and Science (BMBF: Code 01 LL 0918 B). China Scholarship Council supported the research stay of the first author at University of Zurich. We also thank the groups of Bolot Moldobekov from Central-Asia Institute for Applied Geosciences (CAIAG) for supporting our field work in 2010 and 2012. ASTER GDEM and SRTM is a product of METI and NASA. We thank DLR for free access to SRTM X-band data and USGS for free access to SRTM C-band and Landsat data.

Reference

Aizen, V. B., Aizen, E. M., and Kuzmichonok, V. A.: Glaciers and hydrological changes in the Tien Shan: simulation and prediction, Environmental Research Letters, 2, 10.1088/1748-9326/2/4/045019, 2007.

Aizen, V. B., Aizen, E., Dozier, J., and Melack, J. M.: Glacier regime of the highest Tien Shan mountain, Pobeda-Khan Tengry Massif, Journal of Glaciology, 43, 503-512, 1997.

Aizen, V. B., Kuzmichenok, V. A., Surazakov, A. B., and Aizen, E. M.: Glacier changes in the central and northern Tien Shan during the last 140 years based on surface and remote-sensing data, Ann. Glaciol., 43, 202-213, 2006.

Benn, D. I., Bolch, T., Hands, K., Gulley, J., Luckman, A., Nicholson, L. I., Quincey, D., Thompson, S., Toumi, R., and Wiseman, S.: Response of debris-covered glaciers in the Mount Everest region to recent warming, and implications for outburst flood hazards, Earth-Science Reviews, 114, 156-174, http://dx.doi.org/10.1016/j.earscirev.2012.03.008, 2012.

Berthier, E., Arnaud, Y., Kumar, R., Ahmad, S., Wagnon, P., and Chevallier, P.: Remote sensing estimates of glacier mass balances in the Himachal Pradesh (Western Himalaya, India), Remote Sensing of Environment, 108, 327-338, DOI 10.1016/j.rse.2006.11.017, 2007.

Berthier, E., Schiefer, E., Clarke, G. K. C., Menounos, B., and Remy, F.: Contribution of Alaskan glaciers to sea-level rise derived from satellite imagery, Nature geoscience, 3, 92-95, 10.1038/NGEO737, 2010.

Bolch, T., Menounos, B., and Wheate, R.: Landsat-based inventory of glaciers in western Canada, 1985-2005, Remote Sensing of Environment, 114, 127-137, 2010.

Bolch, T., Pieczonka, T. and Benn, D. I.: Multi-decadal mass loss of glaciers in the Everest area (Nepal, Himalaya) derived from stereo imagery, Cryosphere, 5, 349–358, 2011.

Bolch, T.: Climate change and glacier retreat in northern Tien Shan (Kazakhstan/Kyrgyzstan) using remote sensing data, Global and Planetary Change, 56, 1-12, 2007.

Bouillon, A., Bernard, M., Gigord, P., Orsoni, A., Rudowski, V., and Baudoin, A.: SPOT 5 HRS geometric performances: Using block adjustment as a key issue to improve quality of DEM generation, Isprs Journal of Photogrammetry and Remote Sensing, 60, 134-146, http://dx.doi.org/10.1016/j.isprsjprs.2006.03.002, 2006.

Cao, M. S.: Detection of abrupt changes in glacier mass balance in the Tien Shan Mountains, Journal of Glaciology, 44, 352-358, 1998.

Chen, Y., Xu, C., Hao, X., Li, W., Chen, Y., Zhu, C., and Ye, Z.: Fifty-year climate change and its effect on annual runoff in the Tarim River Basin, China, Quaternary International, 208, 53-61, http://dx.doi.org/10.1016/j.quaint.2008.11.011, 2009.

Cuffey, K and Paterson, W. S. B.: The Physics of Glaciers, 4rd ed., Elsevier Sci., New York, 704 pp., 2010.

Ding, Y., Liu, S., Li, J., and Shangguan, D.: The retreat of glaciers in response to recent climate warming in western China, Annals of Glaciology, 43, 97-105, 2006.

Dolgoushin, L. D., & Osipova, G. B.: Glacier surges and the problem of their forecasting. Moscow: Proc. Snow and Ice Symposium (13 pp.), 1975.

Fujita, K., Sakai, A., Nuimura, T., Yamaguchi, S., and Sharma, R. R.: Recent changes in Imja Glacial Lake and its damming moraine in the Nepal Himalaya revealed by in situ surveys and multi-temporal ASTER imagery, Environmental Research Letters, 045205, 10.1088/1748-9326/4/4/045205, 2009.

Gardelle, J., Berthier, E., and Arnaud, Y.: Impact of resolution and radar penetration on glacier elevation changes computed from DEM differencing, Journal of Glaciology, 58, 419-422, 10.3189/2012JoG11J175, 2012.

Gardelle, J., Berthier, E., Arnaud, Y., and Kääb, A.: Region-wide glacier mass balances over the Pamir-Karakoram-Himalaya during 1999-2011, The Cryosphere, 7, 1263-1286, 10.5194/tc-7-1263-2013, 2013.

Gardner, A. S., Moholdt, G., Cogley, J. G., Wouters, B., Arendt, A. A., Wahr, J., Berthier, E., Hock, R., Pfeffer, W. T., Kaser, G., Ligtenberg, S. R. M., Bolch, T., Sharp, M. J., Hagen, J. O., van den Broeke, M. R., and Paul, F.: A Reconciled Estimate of Glacier Contributions to Sea Level Rise: 2003 to 2009, Science, 340, 852-857, 10.1126/science.1234532, 2013.

Glazirin, G. E.: A century of investigations on outbursts of the ice-dammed lake Merzbacher(central Tien Shan), Austrian Journal of Earth Sciences, 103, 171-178, 2010.

Gorokhovich, Y., and Voustianiouk, A.: Accuracy assessment of the processed SRTM-based elevation data by CGIAR using field data from USA and Thailand and its relation to the terrain characteristics, Remote Sensing of Environment, 104, 409-415, http://dx.doi.org/10.1016/j.rse.2006.05.012, 2006.

Hagg, W., Mayer, C., Lambrecht, A., and Helm, A.: Sub-debris melt rates on southern Inylchek Glacier, Central Tian Shan., Geogr. Ann., 90A, 55-63, 2008.

Han, H., Wang, J., Wei, J., and Liu, S.: Backwasting rate on debris-covered Koxkar glacier, Tuomuer Mountain, China, Journal of Glaciology, 56, 287-296, 10.3189/002214310791968430, 2010.

Häusler, H., Scheibz, J., Leber, B., Kopecny, A., Echtler, H., Wetzel, H.-U., and Moldobekov, B.: Results from the 2009 geoscientific expedition to the Inylchek glacier, Central Tien Shan(Kyrgyzstan), Austrian Journal of earth sciences, 104, 47-57, 2011.

Huss, M.: Density assumptions for converting geodetic glacier volume change to mass change, The Cryosphere, 7, 877-887, 10.5194/tc-7-877-2013, 2013.

Jarvis, A., Reuter, H. I., Nelson, A., and Guevara, E.: Hole-filled SRTM for the globe Version 4, available from the CGIAR-CSI SRTM 90m Database (http://srtm.csi.cgiar.org), 2008.

Juen, M., Mayer, C., Lambrecht, A., Haidong, H., and Shiyin, L.: Impact of varying debris cover thickness on ablation: a case study for Koxkar glacier in the Tien Shan, The Cryosphere, 8, 377-386, 10.5194/tc-8-377-2014, 2014.

Kaab, A., Berthier, E., Nuth, C., Gardelle, J., and Arnaud, Y.: Contrasting patterns of early twenty-first-century glacier mass change in the Himalayas, Nature, 488, 495-498, 2012.

Kotlakov, V. M.: World atlas of snow and ice resources, Institute of Geography, Russian Academy of Science, Moscow, 371 pp., 1997.

Krysanova, V., Wortmann, M., Bolch, T., Merz, B., Duethmann, D., Walter, J., Huang, S., Tong, J., Buda, S., and Kundzewicz, Z. W.: Analysis of current trends in climate parameters, river discharge and glaciers in the Aksu River basin (Central Asia), Hydrological Sciences Journal, 10.1080/02626667.2014.925559, 2014.

Leprince, S., Barbot, S., Ayoub, F., Avouac, J. P.: Automatic and precise orthorectification, coregistration, and subpixel correlation of satellite images, application to ground deformation measurements. IEEE Transactions on Geoscience and Remote Sensing, 45(6): 1529-1558, 2007.

Li Jia, L. Z.-W., Wang Chang-Cheng, Zhu Jian-Jun, and Ding Xiao-Li: Using SAR offset-tracking approach to estimate surface motion of the South Inylchek Glacier in Tianshan, Chinese Journal Geophysics, 56, 1226-1236, 2013.

Li, X., Cheng, G., Jin, H., Kang, E., Che, T., Jin, R., Wu, L., Nan, Z., Wang, J., and Shen, Y.: Cryospheric change in China, Global and Planetary Change, 62, 210-218, http://dx.doi.org/10.1016/j.gloplacha.2008.02.001, 2008.

Lifton, N., Beel, C., Hättestrand, C., Kassab, C., Rogozhina, I., Heermance, R., Oskin, M., Burbank, D., Blomdin, R., Gribenski, N., Caffee, M., Goehring, B. M., Heyman, J., Ivanov, M., Li, Y., Li, Y., Petrakov, D., Usubaliev, R., Codilean, A. T., Chen, Y., Harbor, J., and Stroeven, A. P.: Constraints on the late Quaternary glacial history of the Inylchek and Sary-Dzaz valleys from in situ cosmogenic ^{10}Be and ^{26}Al, eastern Kyrgyz Tian Shan, Quaternary Science Reviews, 101, 77-90, http://dx.doi.org/10.1016/j.quascirev.2014.06.032, 2014.

Liu, S. Y., Ding, Y. J., Shangguan, D. H., Zhang, Y., Li, J., Han, H. D., Wang, J., and Xie, C. W.: Glacier retreat as a result of climate warming and increased precipitation in the Tarim river basin, northwest China, Annals of Glaciology, Vol 43, 2006, 43, 91-96, 2006.

Mao, W.Y., Chen, C., Duan, J.J., Su, H.C., Wang, S.F., Wang, J., Ge F.Y.: Streamflow regime of four source streams and mainstream of Tarim River, Xinjiang, in 2000, Journal of Glaciology and Geocryology, 26(4): 488-495, 2004.

Mayer, C., Hagg, W., Lambrecht, A., Helm, A., Scharrer, K.: Post-drainage ice dam response at Lake Merzbacher, Inylchek glacier, Kyrgyzstan. Geografiska Annaler, 90(1): 87-96, 2008.

Narama, C., Kääb, A., Duishonakunov, M., and Abdrakhmatov, K.: Spatial variability of recent glacier area changes in the Tien Shan Mountains, Central Asia, using Corona (~1970), Landsat (~2000), and ALOS (~2007) satellite data, Global and Planetary Change, 71, 42-54, http://dx.doi.org/10.1016/j.gloplacha.2009.08.002, 2010.

Ng, F., Liu, S., Mavlyudov, B., and Wang, Y.: Climateic control on the peak discharge of glacier outburst floods, Geophys. Res. Lett., 34, 10.1029/2007GL0314, 2007.

Nobakht, M., Motagh, M., Wetzel, H.-U., Roessner, S., and Kaufmann, H.: The Inylchek Glacier in Kyrgyzstan, Central Asia: Insight on Surface Kinematics from Optical Remote Sensing Imagery, Remote Sensing, 6, 841-856, 2014.

Nuimura, T., Fujita, K., Yamaguchi, S., and Sharma, R. R.: Elevation changes of glaciers revealed by multitemporal digital elevation models calibrated by GPS survey in the Khumbu region, Nepal Himalaya, 1992-2008, Journal of Glaciology, 58, 648-656, 10.3189/2012JoG11J061, 2012.

Nuth, C., and Kääb, A.: Co-registration and bias corrections of satellite elevation data sets for quantifying glacier thickness change, The Cryosphere, 5, 271-290, 10.5194/tc-5-271-2011, 2011.

Osmonov, A., Bolch, T., Xi, C., Kurban, A., and Guo, W.: Glacier characteristics and changes in the Sary-Jaz River Basin (Central Tien Shan, Kyrgyzstan) – 1990–2010, Remote Sensing Letters, 4, 725-734, 10.1080/2150704x.2013.789146, 2013.

Paul, F., and Haeberli, W.: Spatial variability of glacier elevation changes in the Swiss Alps obtained from two digital elevation models, Geophysical Research Letters, 35, L21512, Doi 10.1029/2008gl034718, 2008.

Paul, F., Barrand, N. E., Berthier, E., Bolch, T., Casey, K., Frey, H., Joshi, S. P., Konovalov, V., Bris, P. L., Molg, N., NOsenko, G., Nuth, C., Pope, A., Racoviteanu, A., Rastner, P., Raup, B., and Scharrer, K.: On the accuracy of glacier outlines derived from remote-sensing data, Ann. Glaciol., 54, 171-182, 10.3189/2013AoG63A296, 2013.

Paul, F., Bolch, T., Kääb, A., Nagler, T., Nuth, C., Scharrer, K., Shepherd, A., Strozzi, T., Ticconi, F., Bhambri, R., Berthier, E., Bevan, S., Gourmelen, N., Heid, T., Jeong, S., Kunz, M., Lauknes, T. R., Luckman, A., Merryman, J., Moholdt, G., Muir, A., Neelmeijer, J., Rankl, M., VanLooy, J., and Van Niel, T.: The glaciers climate change initiative: Methods for creating glacier area, elevation change and velocity products, Remote Sensing of Environment, http://dx.doi.org/10.1016/j.rse.2013.07.043, 2014.

Phil Pressel: Meeting the Challenge: The Hexagon KH-9 Reconnaissance Satellite. American Institute of Aeronautics and Astronautics, Inc., Reston, Virginia, 2013.

Piao, S., Ciais, P., Huang, Y., Shen, Z., Peng, S., Li, J., Zhou, L., Liu, H., Ma, Y., Ding, Y., Friedlingstein, P., Liu, C., Tan, K., Yu, Y., Zhang, T., and Fang, J.: The impacts of climate change on water resources and agriculture in China, nature, 467, 10.1038/nature09364, 2010.

Pieczonka, T., Bolch, T., and Buchroithner, M.: Generation and evaluation of multitemporal digital terrain models of the Mt. Everest area from different optical sensors, Isprs Journal of Photogrammetry and Remote Sensing, 66, 927-940, http://dx.doi.org/10.1016/j.isprsjprs.2011.07.003, 2011.

Pieczonka, T., Bolch, T., Wei, J.unfeng, w., and Liu, S.hiyin, L.: Heterogeneous mass loss of glaciers in the Aksu-Tarim Catchment (Central Tien Shan) revealed by 1976 KH-9 Hexagon and 2009 SPOT-5 stereo imagery, Remote Sensing of Environment, 130, 233–244, 2013.

Quincey, D. J., L.Copland, Mayer, C., Bishop, M., A.Luckman, and Belo, M: Ice velocity and climate variations for Baltora Glacier, Pakistan, Journal of Glaciology, 55, 1061-1071, 2009.

Reyers, M., Pinto, J. G., and Paeth, H.: Statistical–dynamical downscaling of present day and future precipitation regimes in the Aksu River Catchment in Central Asia, Global and Planetary Change, 107, 36-49, http://dx.doi.org/10.1016/j.gloplacha.2013.04.003, 2013.

Rignot, E., Echelmeyer, K., and Krabill, W.: Penetration depth of interferometric synthetic-aperture radar signals in snow and ice, Geophysical Research Letters, 28, 3501-3504, 10.1029/2000gl012484, 2001.

Schomacker, A.: What controls dead-ice melting under different climate conditions? A discussion, Earth-Science Reviews, 90, 103-113, 2008.

Shen,Y.P., Wang, G.Y., Ding, Y.J., Mao, W.Y., Liu, S.Y., Wang, S.D., Duishen M Mamatkanov: Changes in Glacier Mass Balance in Watershed of Sary Jaz-Kumarik Rivers of Tianshan Mountains in 1957—2006 and Their Impact on Water Resources and Trend to End of the 21th Century, Journal of Glaciology and Geocryology, 31, 5, 792-801, 2009[in Chinese with english abstract].

Shi, Y., Shen, Y., Kang, E., Li, D., Ding, Y., Zhang, g., and Hu, R.: Recent and future climate change in northwest China, Climatic Change, DOI 10.1007/s10584-006-9121-7, 2006.

Shortridge, A., and Messina, J.: Spatial structure and landscape associations of SRTM error, Remote Sensing of Environment, 115, 1576-1587, http://dx.doi.org/10.1016/j.rse.2011.02.017, 2011.

Sorg, A., Bolch, T., Stoffel, M., Solomina, O., and Beniston, M.: Climate change impacts on glaciers and runoff in Tien Shan (Central Asia), Nature Climate Change, 2, 725–731, 10.1038/nclimate1592, 2012.

Surazakov, A. B., and Aizen, V. B.: Estimating volume change of mountain glaciers using SRTM and Map-Based Topographic data, IEEE Transactions on Geoscience and Remote sensing, 44, 2991-2994, 2006.

Surazakov, A., and Aizen, V.: Positional Accuracy Evaluation of declassified Hexagon KH-9 Mapping Camera imagery, Photogrammetric Enginneering & Remote Sensing, 76, 1-6, 2010.

Takaku, J., Futamura, N., Iijima, T., Tadono, T., Shimada, M., and Shibasaki, R.: High resolution DEM generation from ALOS PRISM data - simulation and evaluation, Geoscience and Remote Sensing Symposium, 2004. IGARSS '04. Proceedings. 2004 IEEE International, 2004, 4548-4551 vol.4547.

Toutin, T.: Generation of DSMs from SPOT-5 in-track HRS and across-track HRG stereo data using spatiotriangulation and autocalibration, Isprs Journal of Photogrammetry and Remote Sensing, 60, 170-181, http://dx.doi.org/10.1016/j.isprsjprs.2006.02.003, 2006.

Uchiyama, Y., Honda, M., Mizuta, Y., Otsuka, K., Ishizeki, T., Okatani, T., and Tamura, E.: Revising 1:25,000-Scale topographic maps using ALOS/PRISM Imagery, Bulletin of the Geographical Survey Institute, 56, 1-15, 2008.

Unger-Shayesteh, K., Vorogushyn, S., Farinotti, D., Gafurov, A., Duethmann, D., Mandychev, A., and Merz, B.: What do we know about past changes in the water cycle of Central Asian headwaters? A review, Global and Planetary Change, 110, Part A, 4-25, http://dx.doi.org/10.1016/j.gloplacha.2013.02.004, 2013.

USGS: Shuttle Radar Topography Mission, 3 Arc Second scene, Unfilled finished B, Global Land Cover Facility, University of Maryland, College Park, Maryland, February 2000, 2006.

Wang, W., Li, Z., Zhang, G., and Li, X.: The processes and characteristics of mass balance on the Urumqi Glacier No.1 during 1958-2009, Sciences in Cold and Arid Regions, 4, 0505-0513, 10.3724/SP.J.1226.2012.00505, 2012.

WGMS: Fluctuations of Glaciers Database. World Glacier Monitoring Service, Zurich, Switzerland. DOI:10.5904/wgms-fog-2013-11, 2013.

Xu, J., Liu, S., Zhang, S., Guo, W., and Wang, J.: Recent Changes in Glacial Area and Volume on Tuanjiefeng Peak Region of Qilian Mountains, China, PLoS ONE, 8, e70574, 10.1371/journal.pone.0070574, 2013.

Yang, L., Meng, X., and Zhang, X.: SRTM DEM and its application advances, International Journal of Remote Sensing, 32, 3875-3896, 10.1080/01431161003786016, 2011.

Zemp, M., Thibert, E., Huss, M., Stumm, D., Rolstad Denby, C., Nuth, C., Nussbaumer, S. U., Moholdt, G., Mercer, A., Mayer, C., Joerg, P. C., Jansson, P., Hynek, B., Fischer, A., Escher-Vetter, H., Elvehøy, H., and Andreassen, L. M.: Reanalysing glacier mass balance measurement series, The Cryosphere, 7, 1227-1245, 10.5194/tc-7-1227-2013, 2013.

Figure and Table Captions

Figure1 Location and topography of Southern Inylchek Glacier (SIG) and Northern Inylchek Glacier (NIG)

Figure 2 SIG and NIG tongue changes between ~1975 and 2007. The background Landsat TM image was acquired in 1990.

Figure 3 Flow direction and velocity of SIG between 2002 and 2003 (a) and 2010 and 2011 (b)

Figure 4 a: Elevation difference of SIG and NIG between SPOT-5 (2007) and SRTM (1999); b: Elevation difference of SIG and NIG between SRTM (1999) and KH9 (~1975); c: Elevation difference of SIG and NIG between SPOT (2007) and KH9 (~1975). The altitude of points a, b, c, d, and are ~3,080 m a.s.l., ~3,400 m a.s.l., ~3,860 m a.s.l., ~3,430 m a.s.l., ~3,685 m a.s.l., ~4,000 m a.s.l., derived from SRTM. Point a is on the edge of SPOT DEM and ALOS DEM. From the tongue of SIG to point a, the ice elevation differences were derived from ALOS-KH9 in Figure 4a and ALOS-SRTM in Figure 4c. Point c and point e are on the boundary of KH9 in ~1975 and KH9 in 1976.

Figure 5 Longitudinal profiles of SIG and NIG for the period 1975 - 1999 (KH-9-SRTM), 1999 - 2007 (SRTM-SPOT). The section of ALOS between the tongue of SIG and point a was derived from ALOS-SRTM in black line and was derived from ALOS-KH9 in red line.

Figure 6 The annual elevation difference measured for the period of 1975-1999 (KH-9-SRTM) and 1999 - 2007 (SRTM-SPOT) along the elevation zones in the SIG and NIG. For SIG, the elevation difference in zones 2,800-3,000 was derived from ALOS-KH-9 between ~1975 - 2006.

Table 1 List of utilized satellite images and data sources

Table 2 Shift vectors in x, y and z direction (Master DEM->slave DEM) and DEM uncertainty

Table 3 Comparison of GPS points to the SPOT-5 DEM before and after co-registration

Table 4 The SIG and NIG area change between ~1975 and 2007

Table 5 Glacier mass changes based on area-average dh/dt for period ~1975 - 2007.

Table 1 List of utilized satellite images and data sources

Satellite	Time	Pixel size (nadir, m)	Swatch(Km)	B/H	DEM pixel size (m)	Velocity image
ALOS Nadir(N) Backwards(B)	Oct., 08, 2006	2.5	35	0.5	10	-
SPOT-5 HRG	Feb., 05, 2008	2.5	60	0.63	10	-
SRTM Unfilled Finished-B version	Feb., 2000		1°*1°（tile size）	-	90	-
Landsat ETM+	Oct., 13, 1999	15	185	-	-	-
Landsat TM	Sept., 10, 1990	30	185	-	-	-
KH-9 Hexagon	Nov., 16, 1974	6-9	240*120		25	-
KH-9 Hexagon	Jan. 16,1976	6-9	240*120		25	-
Terra ASTER	Aug. 25, 2002	15	60			Yes
Terra ASTER	Aug. 28, 2003	15	60			Yes
Landsat TM	Aug. 16, 2010	30	185			Yes
Landsat TM	Aug. 3, 2011	30	185			Yes

Table 2 Shift vectors in x, y and z direction (Master DEM->slave DEM) and DEM uncertainty

	Shift vectors in x, y and z direction			**Before co-registration With glacier free**		**After co-registation**		**Normalized median absolute deviation(m)**	**Uncertainty(m)**
	X(m)	Y(m)	Z(m)	Mean elevation difference(m)	Standard deviation (STD)(m)	Mean elevation difference(m)	Standard deviation(m)		
SRTM->SPOT	18.7	-46.5	1.3	6.8	20.8	0.4	13.0	1.0	2.1
SRTM->KH-9	34.3	27.3	-5.3	-2.0	18.1	-1.0	15.3	0.5	2.0
SPOT->KH-9	-3.8	22.4	-6.3	-7.7	15.9	-1.4	15.9	1.1	1.1
SRTM->ALOS	23.5	-51.2	6	-6.5	22.3	2.5	10.1	2.1	2.8
ALOS->KH-9	6.2	22.8	-19.5	-12.8	20.5	2.7	19.0	2.3	2.3

Table 3 Comparison with GPS points to the SPOT-5 DEM before and after co-registration

			In stu	DEMs Before co-registration		After co-registration	Description
No	latitude	Longitude	GPS_Elevation(m)	SPOT_DEM(m)	GPS-SPOT ***Difference*** (m)	GPS-SPOT difference(m)	
1	42.22421	79.85953	3351.5	3342.9	8.6	0.8	Glacier free region
2	42.16847	49.8211	3372.4	3358.4	14.0	1.7	Glacier free region
3	42.21839	79.85553	3303.0	3287.0	16	3.6	Debris covered region
4	42.20931	79.84357	3306.3	3287.0	9.3	0.1	Debris covered region
5	42.22095	79.86032	3294.1	3295.0	-0.94	-11.8	Debris covered region
6	42.17129	79.84033	3430.6	3428.4	2.2	3.0	Glacier region

Table 4 The SIG and NIG area change between ~1975 and 2007

	Area(km^2)	Area change							
	~1975	~1975 - 1990		1990 -1999		1999 - 2007		~1975-2007	
		km^2	%	km^2	%	km^2	%	km^2	%
SIG	508.4±6.6	-0.1±0.1	-	-0.5±0.1	-0.1	-0.2±0.1	-	-0.8±0.1	-0.2
NIG	156.6±2.8	-1.2±0.1	-0.8	3.7±0.1	2.4	-0.4±0.1	-0.3	2.0±0.1	1.3

Table 5 Glacier mass changes based on Area-average dh/dt for period ~1975 - 2007

			Altitude zone(m a.s.l.)	Area covered by DEM (km^2)	Percentage of total area (%)	Glacier mass changes (m w.e.a^{-1})
NIG	SPOT-SRTM	1999-2007	3,300-6,400	62.7	39.2	-0.3 ± 0.4
	SRTM-KH9	~1975-1999	3,300-6,300	107.5	67.6	-0.3± 0.1
	SPOT-KH9	~1975-2007	3,400-6,600	109.9	69.1	-0.3 ± 0.1
SIG	SPOT-SRTM	1999-2007	3,000-6,600	241.7	47.6	-0.1± 0.4
	SRTM-KH9	~1975-1999	2,900-6,600	374.5	73.9	-0.5± 0.1
	SPOT-KH9	~1975-2007	2,800-6,600	388.6	76.43	-0.4 ± 0.1

Figure1 Location and topography of Southern Inylchek Glacier (SIG) and Northern Inylchek Glacier (NIG)

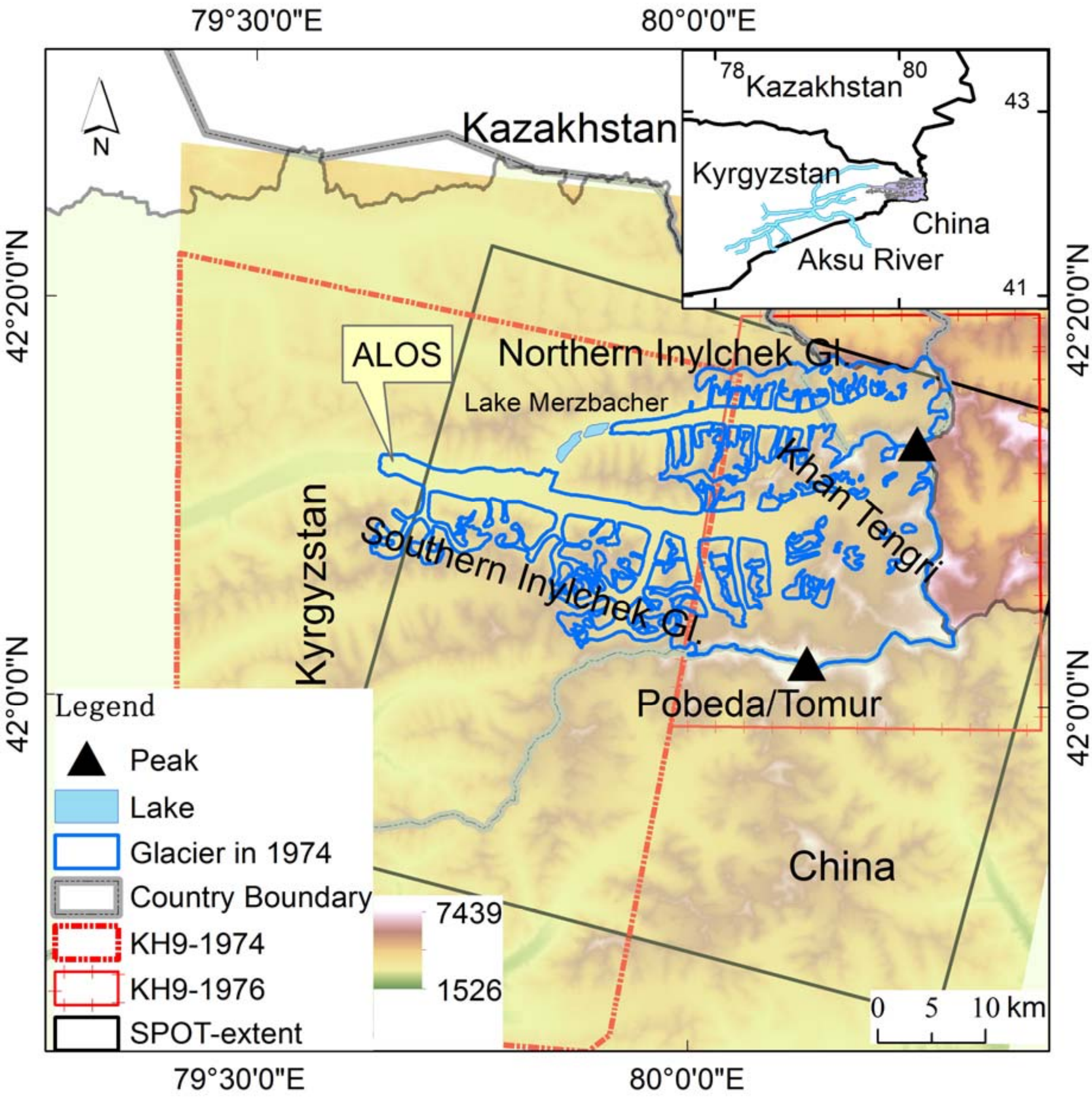

Figure 2 SIG and NIG tongue changes between ~1975 and 2007. The background Landsat TM image was acquired in 1990.

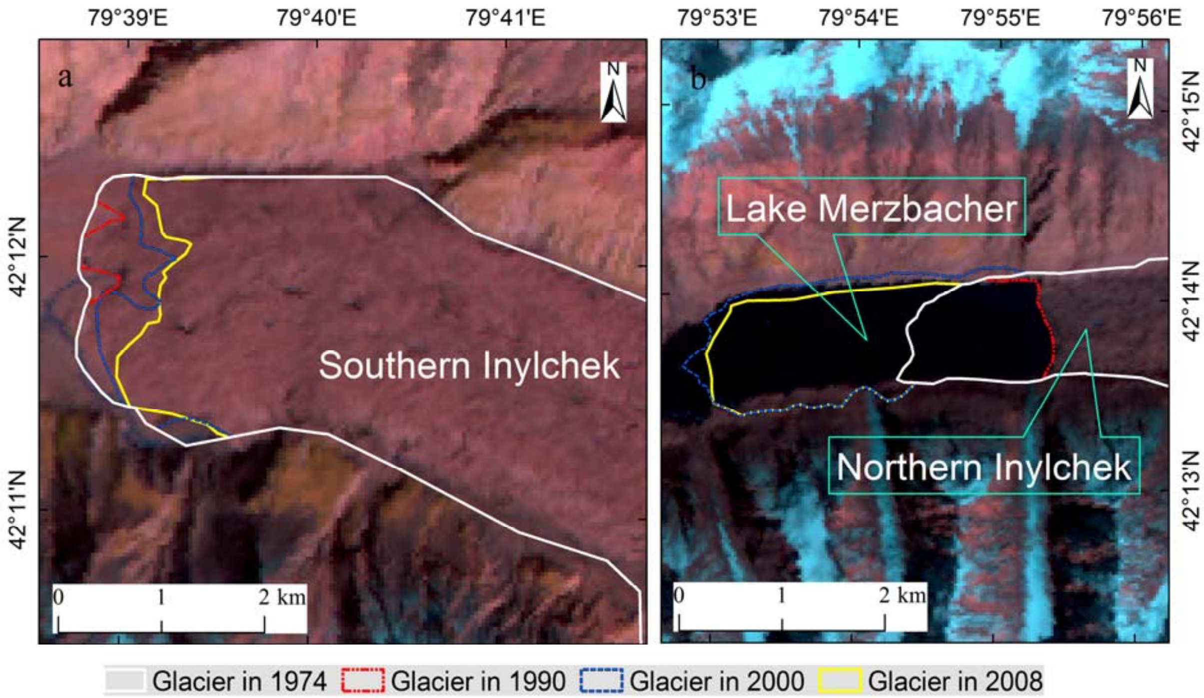

Figure 3 Flow direction and velocity of SIG between 2002 and 2003 (a) and 2010 and 2011 (b)

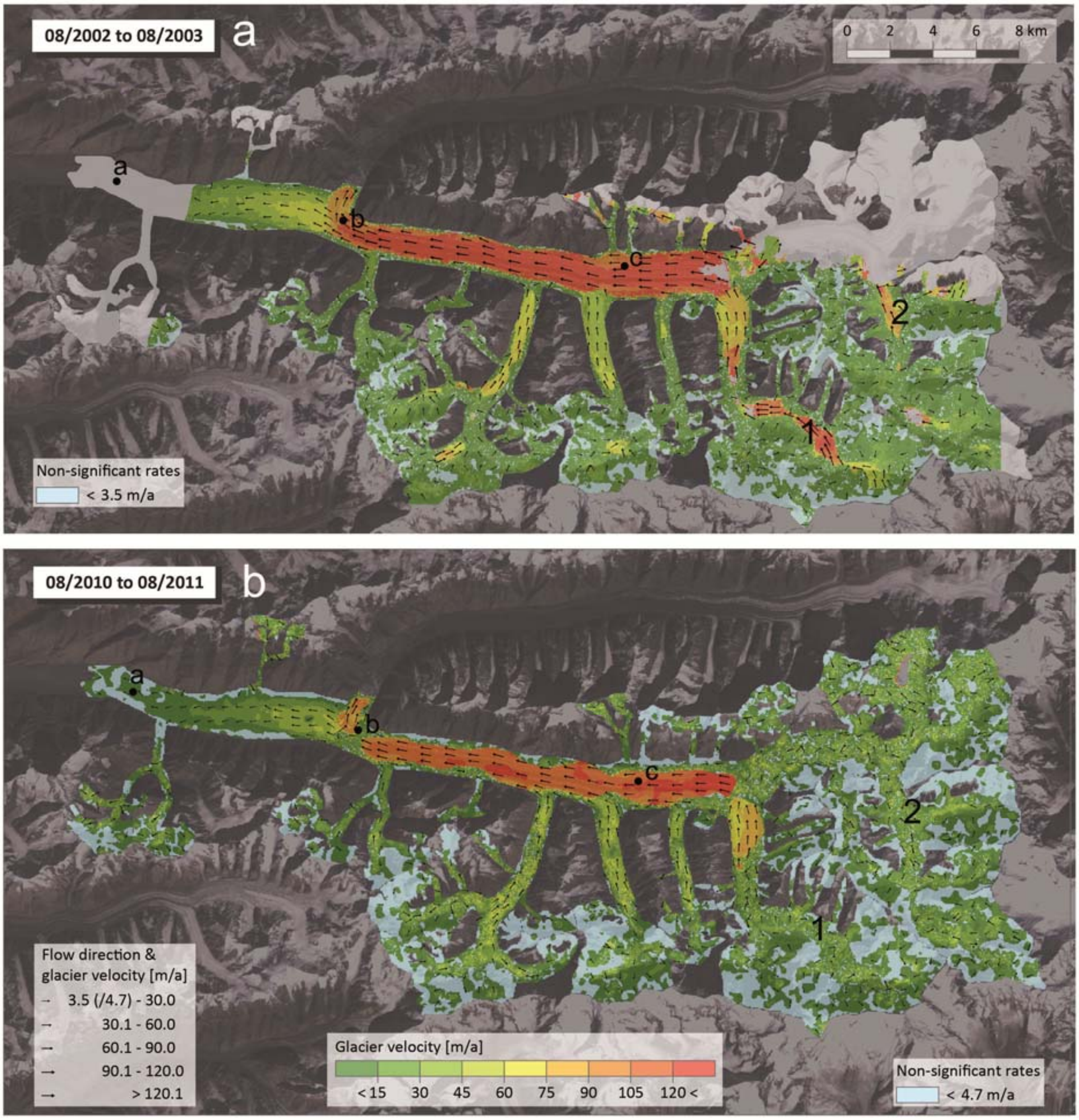

Figure 4 a: Elevation difference of SIG and NIG between SPOT-5 (2007) and SRTM (1999); b: Elevation difference of SIG and NIG between SRTM (1999) and KH9 (~1975); c: Elevation difference of SIG and NIG between SPOT (2007) and KH9 (~1975). The altitude of points a, b, c, d, and are ~3,080 m a.s.l., ~3,400 m a.s.l., ~3,860 m a.s.l., ~3,430 m a.s.l., ~3,685 m a.s.l., ~4,000 m a.s.l., derived from SRTM. Point a is on the edge of SPOT DEM and ALOS DEM. From the tongue of SIG to point a, the ice elevation differences were derived from ALOS-KH9 in Figure 4a and ALOS-SRTM in Figure 4c. Point c and point e are on the boundary of KH9 in ~1975 and KH9 in 1976.

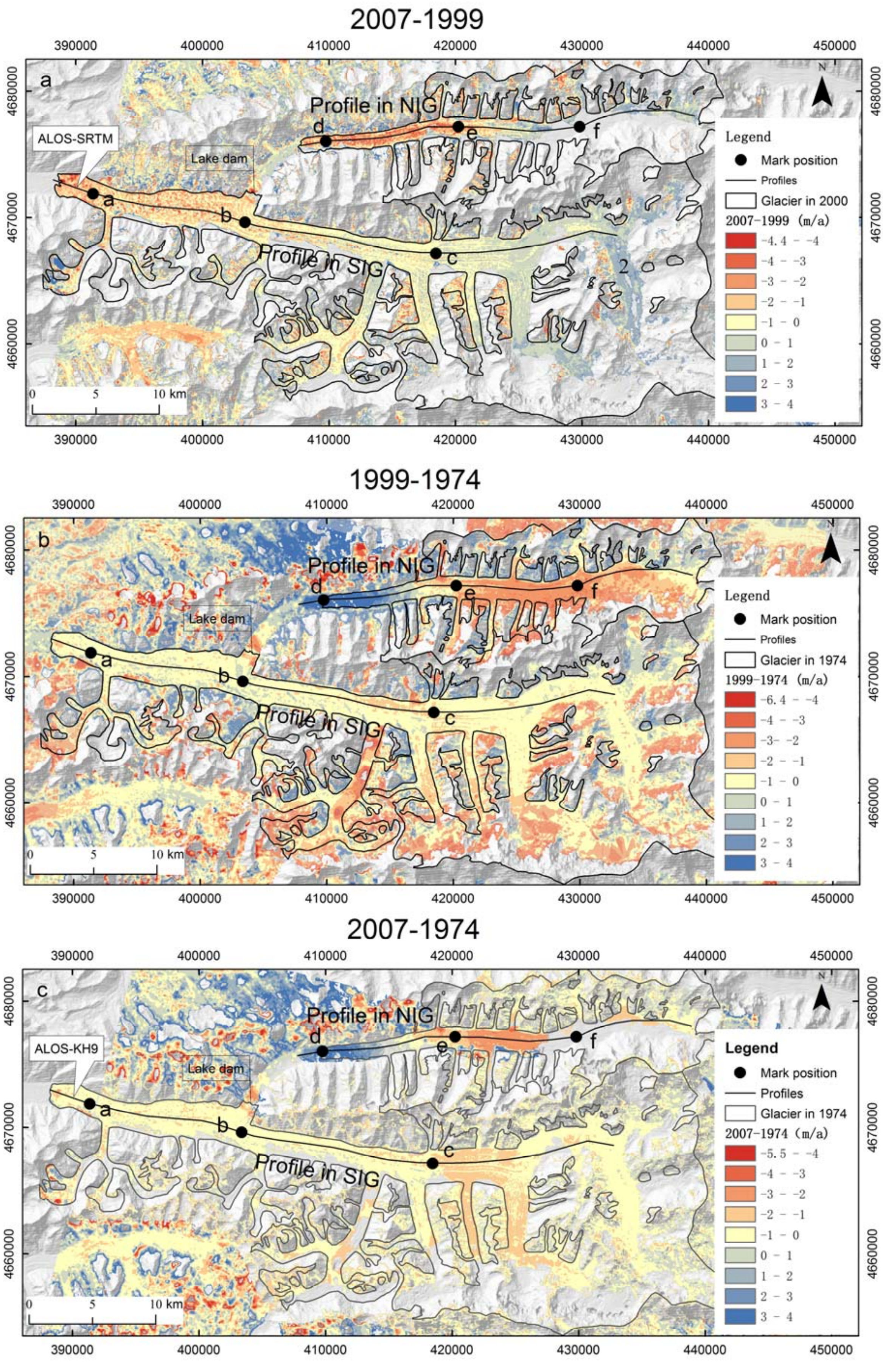
2007-1999
a
ALOS-SRTM
Lake dam
Profile in NIG
Profile in SIG
Legend
Mark position
Profiles
Glacier in 2000
2007-1999 (m/a)
-4.4 - -4
-4 - -3
-3 - -2
-2 - -1
-1 - 0
0 - 1
1 - 2
2 - 3
3 - 4
1999-1974
b
Lake dam
Profile in NIG
Profile in SIG
Legend
Mark position
Profiles
Glacier in 1974
1999-1974 (m/a)
-6.4 - -4
-4 - -3
-3- -2
-2 - -1
-1 - 0
0 - 1
1 - 2
2 - 3
3 - 4
2007-1974
c
ALOS-KH9
Lake dam
Profile in NIG
Profile in SIG
Legend
Mark position
Profiles
Glacier in 1974
2007-1974 (m/a)
-5.5 - -4
-4 - -3
-3 - -2
-2 - -1
-1 - 0
0 - 1
1 - 2
2 - 3
3 - 4
0 5 10 km
390000
400000
410000
420000
430000
440000
450000
4680000
4670000
4660000

Figure 5 Longitudinal profiles of SIG and NIG for the period 1975 - 1999 (KH-9-SRTM), 1999 - 2007 (SRTM-SPOT). The section of ALOS between the tongue of SIG and point a was derived from ALOS-SRTM in black line and was derived from ALOS-KH9 in red line.

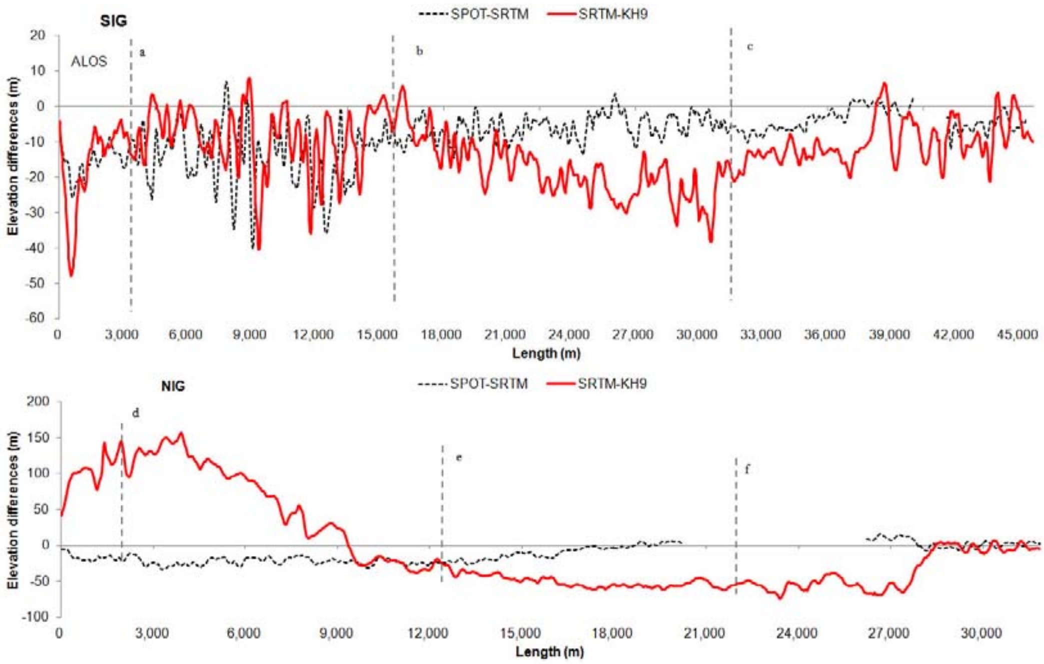

Figure 6 The annual elevation difference measured for the period of 1975-1999 (KH-9-SRTM) and 1999 - 2007 (SRTM-SPOT) along the elevation zones in the SIG and NIG. For SIG, the elevation difference in zones 2,800-3,000 was derived from ALOS-KH-9 between ~1975 - 2006.